10

Related Techniques

As noted previously (chapter 1), PIV developed from Laser Speckle Interferometry. Therefore, one of the early names for this technique was 'Laser Speckle Velocimetry' before 'Particle Image Velocimetry' was established. The Laser Speckle Interferometry (or Laser Speckle Photography) was mainly developed for the determination of displacement and strain in engineering structures. The laser speckles are created due to random interference of scattered light from an optically rough surface illuminated by coherent light. In a pioneering publication Burch & Tokarski [436] showed that, when two such speckle patterns of an object, recorded with and without displacement, are optically transformed, fringes representing the local displacement can be obtained. These fringes, the Young's fringes described in section 5.3, represent the squared intensities of the Fourier Transform of the speckle patterns, which is the power spectrum. An inverse Fourier Transform yields the correlation function of the original image a method which is still the basis for nearly all modern "relatives" of speckle photography.

In contrast to PIV, where lasers are advantageous due to their ability to generate thin and intense light sheets, speckle deformation measurements frequently favor white light illumination. White light speckles instead of laser speckles offer two major advantages: Since laser speckle fields tend to change their appearance when the displacement to be measured exceeds a certain range, the image pairs might de-correlate and the evaluation becomes increasingly difficult. Secondly, the illumination of large and highly three-dimensional objects requires small recording apertures and, as a result of that, powerful and expensive lasers for illumination. Therefore, white light illumination is more frequently used since the 1980's. For this method a speckle pattern, which simply is a random dot pattern sprayed, painted or projected on a background, is generated. The dots should have the highest possible contrast and a spatial frequency that is as high as possible and as small as necessary to be imaged with sufficient contrast. Retroflective paint, consisting of small suspended glass beads for example was used by Asundi & Chiang [433] for contrast enhancement. The technique of pattern projection for wind tun-

nel model deformation measurements has successfully been used by VAN DER DRAAI et al. [441]. Multi-camera systems can be used in order to resolve complex object shapes for the analysis of their topology. The use of pulsed white light sources allows for the observation of moving surfaces. The list of references at the end of the book contains some of the numerous publications on such deformation measurement techniques. From all the various names, the Digital Image Correlation (DIC) apparently became the most common one within the past decade. Therefore, we decided to use the name DIC deformation measurement in the remainder of the book.

However, not only deformations can easily be measured by means of acquisition and evaluation systems similar to PIV, but also density gradients in transparent media. This approach has probably been known since a long time, but it has not drawn much attention until a few years ago. The technique has been referred to as Synthetic Schlieren [438], and Background Oriented Schlieren (BOS) [454] by the different authors. In contrast to the conventional schlieren methods the BOS technique does not require any complex optical devices for illumination. The only optical part needed is an objective lens mounted for instance on a video camera. The camera is focused on a random dot pattern in the background, which generates an image quite similar to a particle image or speckle pattern shown as in figure 10.4. For this reason we refer to this approach as background oriented. Compared to conventional schlieren techniques this procedure results in significantly reduced efforts during its application. However, the optical paths over which the density effects are integrated, are divergent with respect to each other. This can result in a clear disadvantage when large viewing angles have to be used, but is of little influence for recording distances of more than 30 meters used for the tests to be described in section 10.2. In an extension towards Background Oriented Optical Tomography (BOOT), which was proposed by RAFFEL et al. [455], the divergence of the optical paths can be compensated by the evaluation algorithms [443, 447].

Both, the measurement of density gradients in a flow and the detection of the deformation and position of a model in the flow are frequently of interest and can be obtained easily based on PIV imaging hard- and software.

10.1 Deformation Measurement by Digital Image Correlation (DIC)

One of the main motivations for measurements in fluid dynamics is the determination of forces and moments on structures resulting from their interaction with the fluid. Those fluid dynamic forces frequently lead to model deformations and displacements of parts of the setup. Since scaling and shape factors are important experimental parameters, the shape and position of a model have to be monitored repeatedly during the test. Point-wise methods are commonly used for this purpose but are sometimes quite laborious and could miss critical regions. Whole field optical methods can be used for the non-intrusive

measurement of model deformations and displacements. The Moiré Interferometry is one such techniques, which allows obtaining highly accurate results over large fields at once. The disadvantages of the Moiré techniques are their experimental complexity and the fact that the evaluation software, like in many other cases of interferometry, can not always be run fully automatically. Therefore, starting in the 1970'ties correlation based procedures for deformation, displacement, and strain analysis have been developed and applied more and more frequently.

10.1.1 Deformation Measurement in a High-Pressure Facility

Due to the high costs and a limited feasibility of complex laser measurements at full-scale test conditions, most experimental studies on the aerodynamics of high-speed trains are conducted on sub-scales in wind tunnel facilities. However, in most cases the Reynolds and Mach numbers of the model investigations do not match the full-scale vehicle at the same time. Most modern low-speed wind tunnels reach appropriate Mach numbers of $0.1 < Ma < 0.3$. However, if the relative air speed is approximately the same for both the model and the full-scale train, the Reynolds number in the wind tunnel will obviously be much smaller than that of the full-scale vehicle. For aerodynamically well-designed configurations, the resulting mismatch in Reynolds number leads to a certain discrepancy of measured drag and moment values. This brings facilities into play, which are specialized for high Reynolds number investigations like high-pressure facilities. Those facilities allow for the realization of the relevant Mach and Reynolds numbers at reduced scales. Since loads on the model increases with increasing pressure, model deformations and deflections have to be monitored carefully during tests.

The high-pressure wind tunnel of DNW (HDG), shown in figure 10.1, is a closed circuit low-speed wind tunnel, which can be pressurized up to 100 bar. The dimensions of the test section are $0.6 \times 0.6\,\mathrm{m}^2$ with a length of 1 m. 1 : 50 and 1 : 66 models are usually used in order to realize a blockage ratio below 10%. With the maximum speed of 35 m/s and a maximum pressure of 100 bar the achieved Reynolds number is of the same order of magnitude as the full-scale one (e.g. $Re = \mathrm{O}[10^7]$). The flow remains incompressible over the whole range of Reynolds numbers.

The model of the lead car and the first part of the trailer of a train shown in figure 10.2, are designed to carry a six-component internal balance. The strain gage balance is relatively compact and measures forces up to approximately 1000 N. All components of force and moment are available and have been measured for a range of yaw angles between $-30° < \beta < +30°$ during these tests. The lead vehicle and the trailer were mounted sidewards onto the sting.

Digital Image Correlation (DIC) has been applied to generic high-speed train models in order to measure model deflections and model deformations due to wind load. The stiffness of models in high-pressure wind tunnels is generally more critical since their dimensions are smaller and the wind loads are

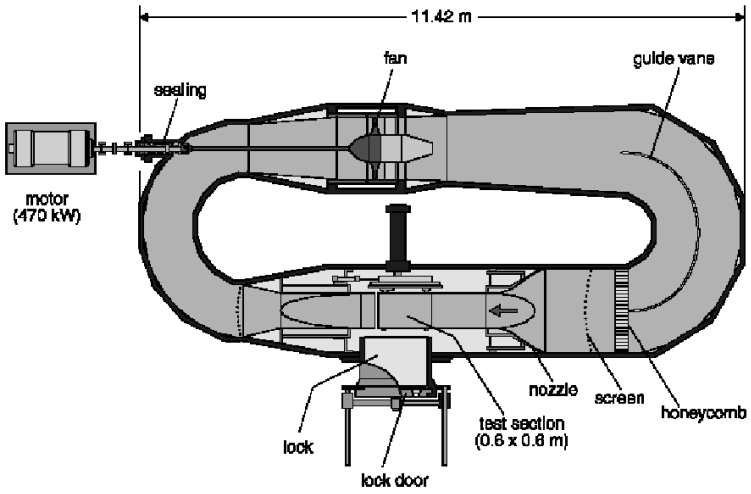

Fig. 10.1. Sketch of the high pressure wind tunnel (HDG) of DNW.

higher as compared to conventional wind tunnels. As mentioned previously, DIC is basically an image processing technique that calculates the displacement of a random dot pattern – which is somehow attached or projected onto the object under investigation – by using correlation techniques. Today, the digital correlation algorithms used for DIC, BOS and PIV are robust and offer small relative errors below 0.1%. In the case of the model deformation measurements presented here, DIC allows for the determination of small deformations with standard deviations of approximately 0.1 pixel of the CCD-sensor

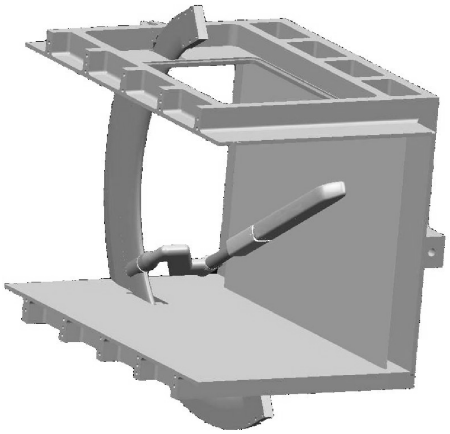

Fig. 10.2. Sketch of the train model configuration in the test section of the HDG.

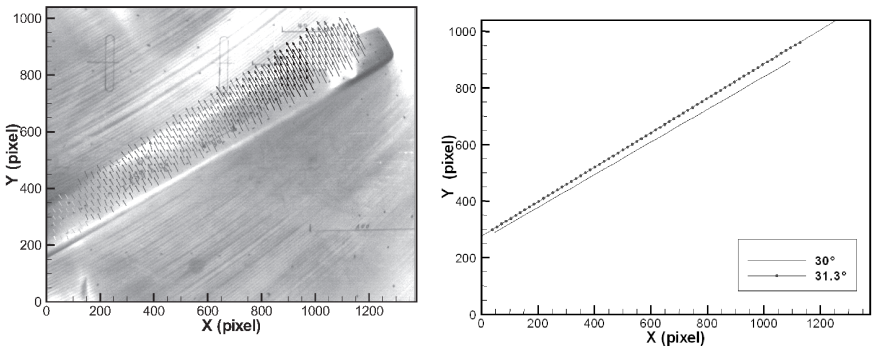

Fig. 10.3. Instantaneous DIC result, showing the local displacement vectors gray leveled by their magnitude (left) and the measured positions of the random dots at $\alpha = 30°$ reference recording (straight line) and the positions measured under wind load at $P_0 = 30\,\text{bar}$ and $U_\infty = 20\,\text{m/s}$ (dotted line) (right).

used. This corresponds to a 0.01 mm accuracy for this measurement of the position of the train model in the HDG wind tunnel. The model – on which a random dot pattern of black ink has been painted – was mounted on a sting and equipped with an internal six component balance (figure 10.2). An additional ground plate was mounted in order to cut off the wind tunnel boundary layer and to ensure well-defined boundary conditions. The plate was parallelized to the wind tunnel floor by measuring the pressure distribution in the center (at yawing angles of $\beta = 0°$). Force measurements were performed in the high-pressure wind tunnel and the DIC technique was applied in order to correct the yawing angle. It can easily be seen in figure 10.3, that in spite of the very stiff sting and support, the yawing angle of the model was significantly changing depending on the free stream velocity (e.g $\pm 1.3°$ at 20 m/s).

Figure 10.3 shows an example of instantaneous pattern correlations on the left hand side. One hundred vector fields were used to process the mean angle shown on the right of figure 10.3. It can be seen that the displacement increases linearly due to sting bending. Additional model deformations, which would result in more complex displacement patterns, were not observed. In the way the DIC technique was applied here, only deformations in the $x - z$-plane could be determined. However, generally this technique is well-suited for three-dimensional measurements if two or more cameras are used [24].

10.2 Background Oriented Schlieren Technique (BOS)

10.2.1 Introduction

Optical density visualization techniques such as schlieren photography, shadowgraphy or interferometry are well known and have been used world wide for

many decades. The techniques are sensitive to changes of the refractive index caused by the variations in the fluid density. Even though some researchers have performed large-field and focusing schlieren photography and shadowgraphy in the great outdoors (e.g. [435], [459], [466]), most of these techniques are confined to laboratories or to wind tunnels and they are less suitable for large- or full-scale applications. Nevertheless, full-scale measurements are desirable if the flow is strongly dependent on Mach and Reynolds numbers. This section describes a technique which determines density gradients without using any sophisticated optical equipment. The technique has been successfully applied to a helicopter in hovering flight and to the transonic flow behind a cylinder.

10.2.2 Principle of the BOS Technique

The Background Oriented Schlieren technique is based on the relation between the refractive index of a gas, n, and the density, ρ, given by the Gladstone-Dale equation, $(n-1)/\rho = const$. It can best be compared with laser speckle density photography as described by Debrus et al. [439] and Köpf et al. [449] and in improved versions by Wernekinck & Merzkirch [465] and Viktin & Merzkirch [464]. Like interferometry, the laser speckle density photography relies on an expanded parallel laser beam, which crosses through a transonic flow field or – in more general terms – through an object of varying refractive index (i.e. a phase object). However, in contrast to interferometry, laser speckle patterns are generated instead of interference fringes. Since white light based techniques for the determination of fluid density gradients are frequently called schlieren[1] techniques [19], the technique described in this chapter will be referred to as the background oriented schlieren technique. Compared to the optical techniques mentioned above, the BOS method simplifies the recording. The speckle pattern, usually generated by the expanded laser beam and ground glass, is replaced by a random dot pattern on a surface in the background of the test volume. This pattern has to have a high spatial frequency that can be imaged with high contrast.

Usually, the recording has to be performed as follows: first a reference image is generated by recording the background pattern observed through air at rest in advance or subsequent to the experiment. In the second step, an additional exposure through the flow under investigation (i.e. during the wind tunnel run) leads to a displaced image of the background pattern. The resulting images of both exposures can then be evaluated by correlation methods. Without any further effort existing evaluation algorithms, which have been developed and optimized for example for particle image velocimetry (or other forms of speckle photography) can then be used to determine speckle displacements. As stated previously, the deflection of a single beam contains

[1] The German word "Schliere" designates a local optical inhomogeneity in a transparent medium.

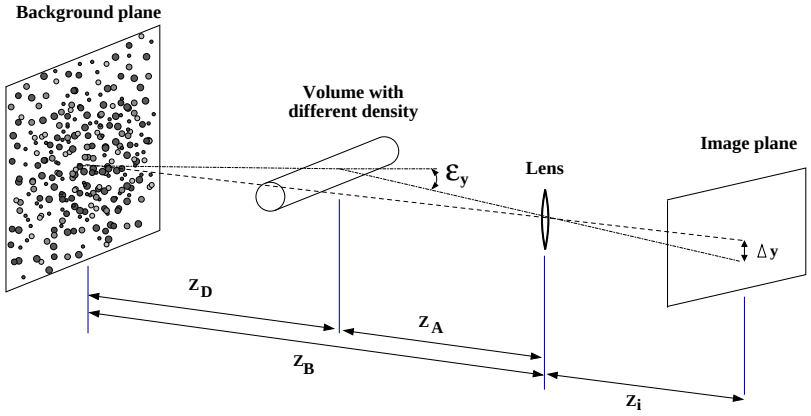

Fig. 10.4. Sketch of a BOS setup.

information about the spatial gradient of the refractive index integrated along the line of sight (see figure 10.4). Details on the theory of ray tracing through gradient-index media could be found in [461] and [440].

The idea of the BOS method is to simplify the optical arragement by replacing the laser speckle with a random dot pattern, which may simply consist of ink or paint droplets, splashed onto a background surface (see figure 10.4). The background pattern may also be generated by a print of a single exposed image of tracer particles.

Assuming paraxial recording and small deflection angles, a formula for the image displacement Δy can be derived, which is valid for density speckle photography as well as for the BOS technique.

$$\Delta y = Z_D M \varepsilon_y \tag{10.1}$$

with the magnification factor of the background, $M = z_i/Z_B$, the distance between the dot pattern and the density gradient, Z_D, and

$$\varepsilon_y = \frac{1}{n} \int \frac{\partial n}{\partial y} dz \tag{10.2}$$

The image displacement Δy can thus be rewritten as

$$\Delta y = f \left(\frac{Z_D}{Z_D + Z_A - f} \right) \tag{10.3}$$

with Z_A being the distance from the lens to the object and the focal length of the lens, f. Since the imaging system has to be focused onto the background; we note:

$$\frac{1}{f} = \frac{1}{z_i} + \frac{1}{Z_B} \tag{10.4}$$

Equation (10.4) shows that a large image displacement can be obtained for a large Z_D and small Z_A. The maximum image displacement for Z_D approaches $\Delta y = f \cdot \varepsilon_y$. On the other hand certain constraints in the decrease of Z_A have

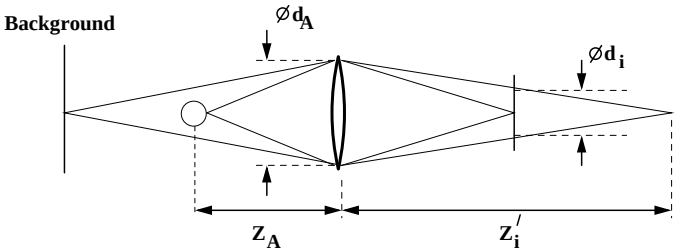

Fig. 10.5. BOS focusing position and image blur.

to be fulfilled in order to image the flow field sufficiently sharply. The optical system has to be focused on the background in order to obtain maximum contrast at high spatial frequencies for later interrogation, and equation (10.4) applies. On the other hand, the sharp imaging of the density gradients would be best at z_i with

$$\frac{1}{f} = \frac{1}{z_i'} + \frac{1}{Z_A} \tag{10.5}$$

By introducing the aperture diameter d_A and the magnification of the density gradient imaging $M' = z_i'/Z_A$ a formula for the blur d_i (see also figure 10.5) of a point at Z_A reads:

$$d_i = d_A \left(1 + \frac{1}{f} M'(f - Z_A)\right) \ . \tag{10.6}$$

Since correlation techniques average over the interrogation window area, the image blur d_i does not lead to a significant loss of information, as long as d_i is considerably smaller than the interrogation window size.

10.2.3 Application of the BOS to Compressible Vortices

Rotor Tip Vortices

The background oriented technique was successfully applied to study different types of flows [454, 438]. In this section two experiments are presented: A helicopter blade tip vortex investigation and an investigation of the wake behind a cylinder. First tests were performed in order to verify the feasibility of BOS for large-scale aerodynamic investigations. The subject helicopter – a Eurocopter BK117 – departed from the ground of DLR in Göttingen. Progressive scan CCD cameras, with a resolution of 1280 × 1024 pixel at 8 frames per second, were previously mounted in a window of a building at a horizontal distance of 32 m from the helicopter and 11.2 m above the ground. A random dot pattern was generated by splashing tiny droplets of white wall paint (between 1 and 10 mm diameter) with a brush onto the concrete ground. More than 50 digital images were recorded within 20 seconds of hover flight.

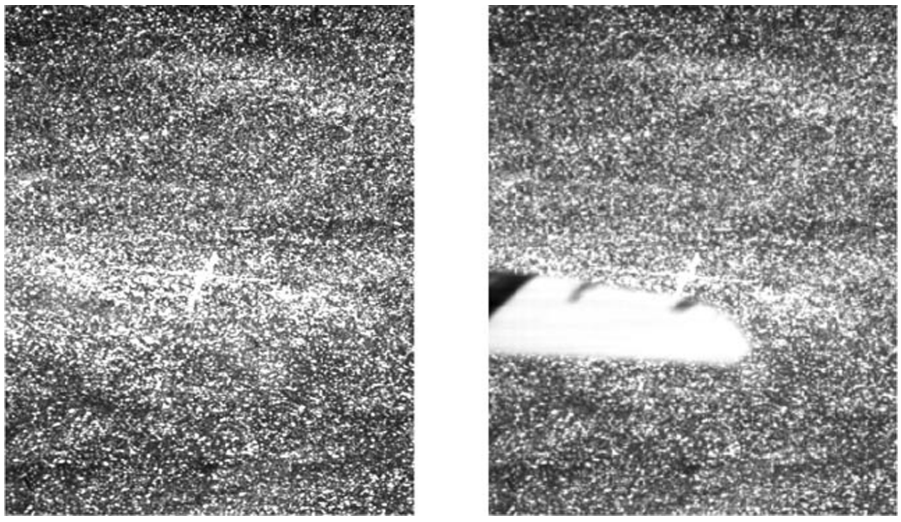

Fig. 10.6. An example of a BOS reference-data image pair at the blade tip of a helicopter in hover flight, see the text for details.

The exposure time was set to 100 μs. The reference recordings were made directly after the departure of the helicopter. Figure 10.6 shows an example of an image pair. The left-hand side shows the reference image, which was recorded after the departure of the helicopter. The right-hand side of figure 10.6 shows the corresponding BOS image with the blade tip (moving at approximately 280 m/s).

Even though acceptable results could be obtained by using a standard cross-correlation displacement measurement software, as developed for PIV, more sophisticated programs helped to adapt the peak-fitting routine to the size of the dot images. The best results were obtained by using an iterative Levenberg-Marquardt fit to a 10×10 pixel area, where the correlation values are weighted according to the Fisher transform (for details see [155]). The size of the interrogation window was 20×20 pixel, corresponding to 2.4 by 1.8 cm in the rotor plane, localized in a window of 64×64 pixel. The evaluation led to the vector plots shown in figure 10.7, which were obtained by a massive oversampling using a five-pixel step-width, resulting in an improved visibility of the flow structures under investigation.

In figure 10.7 (left-hand side), the young vortex shedding from the blade that has just passed the observation area can easily be detected as well as the vortices generated by previous blades. After their generation, the blade tip vortices do not dissipate or diffuse for many rotor revolutions. The perspective projection led to an elliptical appearance of the vortex axes in the image plane. The line of lower density, which can be defined as the vortex center, is also clearly visible on the zoom view (right hand side). Since the cameras were not synchronized with the helicopter rotor blades, the blades do not appear on

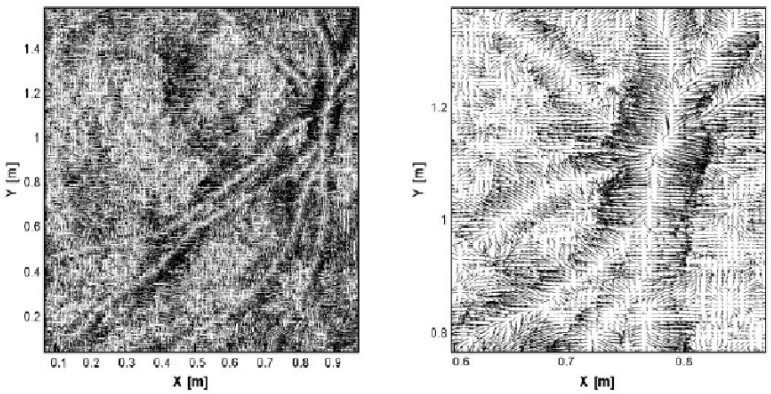

Fig. 10.7. BOS results showing vectors of the measured displacement field which are proportional the density gradients in the helicopter tip vortices.

all recordings and it is therefore impossible to distinguish between the vortex generated by the blade just passing and the vortices from previous blades. If the vortices are overlapping on the camera's field of view, the BOS technique does not allow us to obtain a defined path.

Cylinder Wake Flows

The experiment described next was set up in order to study compressible vortex flows involved in the blade vortex interaction (BVI) phenomena of helicopter rotors in more detail. Therefore, the vortex shedding on a cylinder with a diameter of $d = 25\,\mathrm{mm}$ in a transonic wind tunnel – the VAG of DLR in Göttingen – has been investigated by simultaneous velocity and density gradient measurements at different free-stream Mach numbers. This information was complemented by additional measurements of the unsteady pressure fluctuations at different locations along the wind tunnel walls. These data enable a more detailed analysis of compressible vortices than successive measurements of single quantities. In addition, a detailed description of compressible vortices plays a key role in numerical simulations, which aim at further improvements in the prediction of helicopter noise emissions. The measurement of the velocity induced by the vortex is needed, since the amplitude of the pressure fluctuations which are emitted from the interaction of the vortex with a blade is proportional to the circulation, Γ, of the vortex. In the past, the velocity information has been derived by simultaneous pressure and density measurements (see e.g. [451]). Therefore, one had to assume the vortex to move at a constant convection velocity, that it is symmetric with respect to its axis and that the vortex can be described by a solution of the stationary Euler equations, that is, disregarding the effects of dissipation. Even if thoseassumptions were justified, they definitely limit the accuracy of

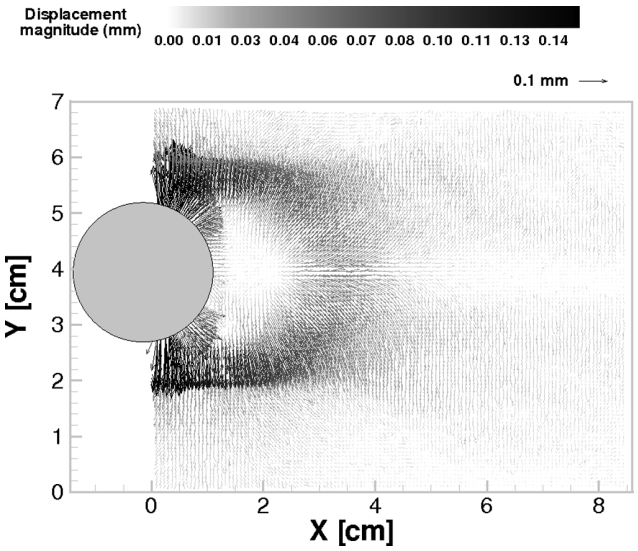

Fig. 10.8. Density gradients obtained with a long exposure time at Ma=0.79.

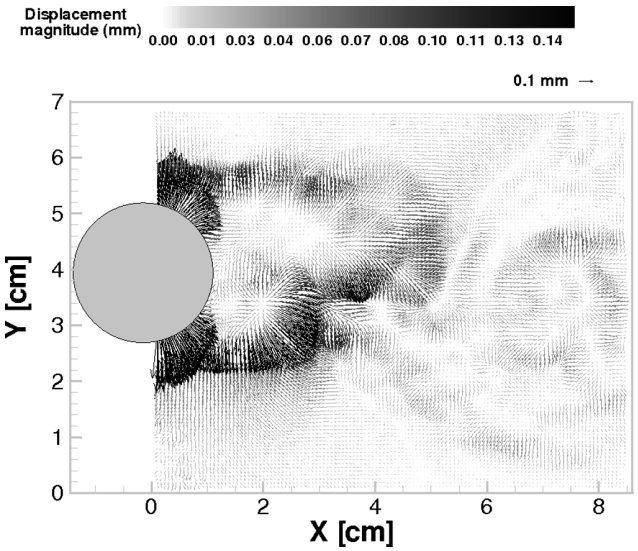

Fig. 10.9. Density gradients obtained with a short exposure time at Ma=0.79.

the experimental results. Furthermore, the spatio-temporal derivatives of the pressure signal, which have to be computed in order to derive the induced velocities, amplify the noise and uncertainty of the data.

The situation can be improved by simultaneous measurements of pressure, density and velocity fields. The setup needed for the BOS measurements was composed of one camera looking through the test section and a light source, which illuminates a background paper containing a dot pattern (figure 10.4). The dot pattern was generated by printing a single exposure PIV recording on a laser printer. The size of the dots was approximately 1 mm and the size of

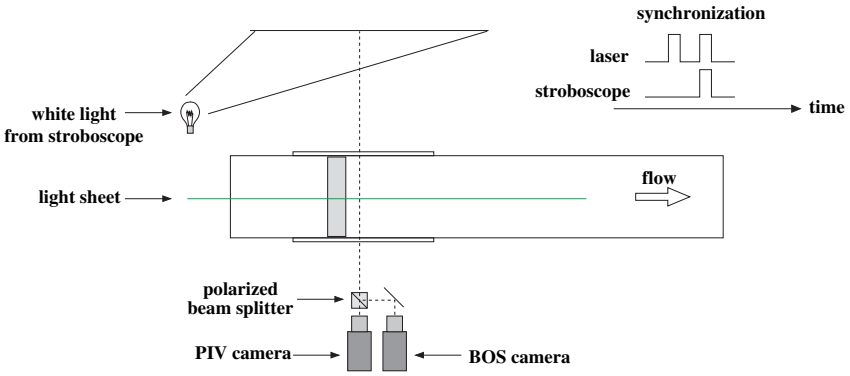

Fig. 10.10. Optical setup for simultaneous PIV and BOS measurements.

the interrogation window backprojected into the observation area was 25 mm^2 on average.

Two different light sources were used: a continuous white light and a stroboscope light synchronized with the camera. The results which are shown first represent the averaged density field and were obtained with continuous light. Figure 10.8 shows displacement fields using continuous light at $Ma = 0.79$. The region of the shear layers above and below the cylinder can clearly be detected on the density gradient field for a Reynolds number of $Re = 335000$. Intermittent compression shock waves (expected at Ma=0.6 ... 0.8), however, could not be observed due to smearing effects of long exposures. However, the strong density gradients and the expected decrease of density behind the cylinder can clearly be seen at this Reynolds number (cp. figure 10.11). The unsteadiness of the vortex wake for this set of parameters becomes visible when comparing averaged and instantaneous results (Fig. 10.8 and Fig. 10.9). This demonstrates the need of instantaneous measurements and made simultaneous velocity and density gradient fields desirable, which will be described further below.

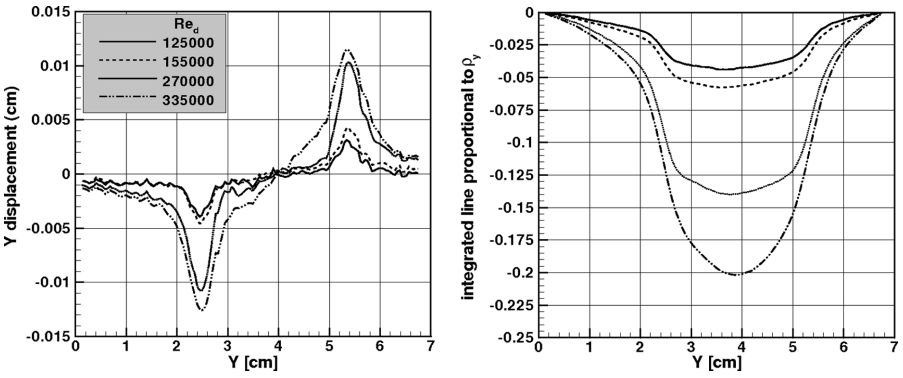

Fig. 10.11. BOS density gradient distributions (left) and their integration to density distributions (right).

The displacement field can be integrated in order to obtain a distribution which is proportional to the density distribution assuming a two-dimensional flow field. Two integration methods can be used: either by solution of the Poisson equation [456] or by line integration. The second method which is the simplest to implement, has the disadvantage of producing line noise. Figure 10.11 shows the line extracted (left hand side) from the time averaged displacement fields for different Reynolds numbers at $x = 1.5\,\mathrm{cm}$ and the result after integration (right hand side). It can be seen that the displacement increases while the density decreases with Reynolds number and shows an almost perfect symmetry in relation to the center of the cylinder with a lowest density for $y = 4\,\mathrm{cm}$. The cylinder diameter has been chosen in order to restrict the ratio between cylinder diameter, d, and its span, s, to $d/s = 1/4$. As can be seen by comparing averaged and instantaneous results (figure 10.8 and 10.9), the vortex wake for this set of parameters is highly unsteady. This demonstrates the need for instantaneous measurements and makes simultaneous velocity and density gradient fields desirable. The advantage of the BOS technique is that it can very easily be coupled with PIV.

Figure 10.10 shows the setup needed to perform BOS and PIV measurements at the same time, which allows for obtaining simultaneous velocity and density data. It is composed of two cameras, one used for PIV and the other for BOS. Both cameras have the same field of view and are looking through a polarized beam splitter, which blocks the light from the laser sheet for the BOS camera. The PIV camera was focused on the laser light sheet plane, whereas the BOS camera was focused onto the background dot pattern. The stroboscope light was synchronized with the second pulse of the laser. The background of the second image is therefore brighter than the first, but the quality of the correlation data was not significantly reduced.

Figure 10.12 shows a zoom of a region where a vortex is visible: in the BOS result, the vectors are diverging from the center of the vortex, which corresponds to an area of lower density.

10.2.4 Conclusions

The measurements demonstrate the feasibility of the BOS technique for different applications – even large-scale ones – by visualizing the blade tip vortices of a helicopter in flight. It is expected that geometry parameters such as the location of the vortex relative to the rotor plane, the orientation of the vortex axis in space and its strength can be derived [448]. In spite of the difficult experimental conditions density gradient data were obtained, which allows for the visualization of density fields with quite a promising spatial resolution. Compared to previous measurements, the time needed for the setup and for data acquisition can be considerably decreased. However, since a single camera system is capable of measuring only two components of the spatial density gradient integrated along the optical path, further information on the position or orientation of the vortex axis in three-dimensional space cannot be derived

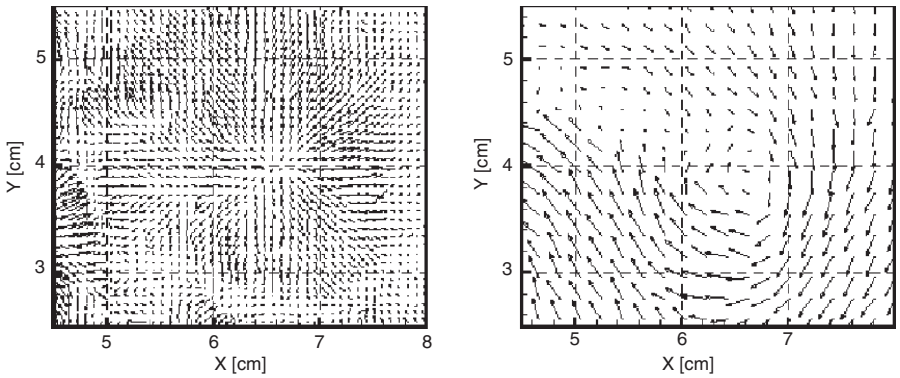

Fig. 10.12. Sample result of simultaneous BOS (left) and PIV (right) data of a cylinder wake flow.

without changing the viewing direction. Assuming a radially symmetric density distribution in the vortex, the use of a second camera in a stereoscopic arrangement would allow the determination of the location of the density gradient in space. After having demonstrated the feasibility of the concept by its application to a technologically relevant but fluid mechanically complex problem, more detailed studies of vortices behind a cylinder were performed in order to reduce the complexity of the vortical structures under investigation and to perform simultaneous velocity measurements. Those measurements will allow a more accurate modeling of vortices in future aero-acoustic prediction codes for helicopters. Furthermore, BOS renders full-scale in-flight rotor tip vortex morphology studies possible by relying on fairly simple sensor units in combination with natural formation backgrounds. Moreover, tomographic BOS data evaluation enables airborne vortex core density estimations [447].